IAES International Journal of Robotics and Automation (IJRA)
Vol. 14, No. 4, December 2025, pp. 345~355
ISSN: 2722-2586, DOI: 10.11591/ijra.v14i4.pp345-355

A method integral sliding mode control to minimize chattering in sliding mode control of robot manipulator

Mai Hoang Nguyen, Truc Thi Kim Nguyen
Faculty of Electrical Engineering, Danang University - University of Science and Technology, Danang, Vietnam

Article Info

Article history:

Received Jan 12, 2025
Revised Aug 1, 2025
Accepted Aug 26, 2025

Keywords:

Adaptive gain
Boundary layer
Chattering suppression
Robotic manipulator
Sliding mode control

ABSTRACT

This paper presents an improved sliding mode control (SMC) strategy for robotic manipulators by introducing a novel exponential integral-based adaptive gain law, referred to as integral sliding mode control (ISMC). The proposed approach dynamically adjusts the switching gain KKK in real-time, based on the accumulated system error, thereby effectively reducing chattering while preserving system robustness. Unlike many existing methods, the ISMC strategy eliminates the need for state observers or complex estimation techniques, simplifying implementation. Theoretical analysis is provided using Lyapunov stability theory, ensuring global convergence. Simulation results on 2-DOF and 3-DOF robotic arms demonstrate superior tracking accuracy and smoother control signals compared to conventional SMC approaches. This work contributes a lightweight yet effective SMC enhancement with practical benefits for real-world robotic applications.

This is an open access article under the CC BY-SA license.

Corresponding Author:

Mai Hoang Nguyen
Faculty of Electrical Engineering, Danang University - University of Science and Technology
Danang, Vietnam
Email: nhmai@dut.udn.vn

1. INTRODUCTION

Sliding mode control (SMC) is a well-established robust control technique, celebrated for its ability to ensure high performance despite nonlinearities, model uncertainties, and external disturbances [1]–[3]. Its discontinuous control action guarantees finite-time convergence to a desired trajectory, making it particularly attractive for high-precision applications like robotic manipulators [4], [5]. However, the discontinuous nature of SMC often induces the chattering phenomenon, which manifests as high-frequency oscillations in the control signal. Chattering can lead to mechanical wear, excitation of unmodeled dynamics, and degraded overall system performance [4]. This issue has become a central focus in the design of control systems for robotic manipulators, where smooth and precise operation is essential [6], [7].

Early approaches to mitigate chattering involved replacing the discontinuous sign function with continuous approximations, such as the boundary layer method, which introduces a thin boundary layer around the sliding surface [8], [9]. Although these continuous approximations reduce chattering, they often involve a trade-off between robustness and accuracy. Higher-order sliding mode controllers, like the super-twisting algorithm, have been proposed to balance these trade-offs, providing both fast convergence and chattering reduction [3], [10]. However, these methods can be complex and typically require precise knowledge of system dynamics [11].

To further address these challenges, adaptive and intelligent control strategies have been explored. These methods integrate fuzzy logic and neural networks into SMC frameworks to improve real-time adaptability and robustness in dynamic environments [6], [12]–[20]. Model-free adaptive control (MFAC) [4], [6],

[10], [13], [15] and dual-projection MFAC [13] have emerged as promising alternatives that eliminate the need for detailed system models, enhancing the practicality of SMC in uncertain environments. Fractional-order and terminal sliding mode controllers have also been introduced to ensure fast convergence and robustness while mitigating chattering in complex nonlinear systems [10], [15], [16], [21].

Recent studies have also focused on observer-based SMC and disturbance observer techniques, which estimate and compensate for unknown dynamics, thereby reducing reliance on high control gains that exacerbate chattering [12], [14], [16]. Time-delay estimation and reinforcement learning have been incorporated to adaptively optimize control policies and minimize chattering while maintaining robustness [10], [13], [22]–[26]. These advancements have been successfully applied in various real-world scenarios, including underwater vehicles, exoskeleton robots, and aerial manipulators [14], [27]–[29].

Integral sliding mode control (ISMC) has recently emerged as a particularly promising extension of SMC [10], [15]. By eliminating the reaching phase, ISMC ensures continuous robustness from the initial state onward, making it suitable for high-precision tasks in dynamic and uncertain environments. Recent ISMC developments have integrated adaptive gain tuning, disturbance estimation, and intelligent optimization algorithms (*e.g.*, neural networks, fuzzy logic, or particle swarm optimization), showing further improvements in chattering suppression and tracking performance [16], [22], [30]–[32].

Despite these advancements, challenges remain in achieving an optimal balance between chattering suppression and robust performance [33], [34]. Many adaptive and intelligent SMC methods require complex computations and precise system modeling, which may not be feasible in real-time applications [15], [17], [35]. Motivated by these challenges, this paper proposes an ISMC strategy that combines adaptive gain tuning with a boundary layer method. The proposed ISMC approach adjusts the control gain adaptively based on an exponential integral of the tracking error, while the boundary layer ensures smoother control actions to reduce chattering. The effectiveness of the proposed ISMC strategy is validated through simulations and experiments on 2-DOF and 3-DOF robotic manipulators, demonstrating significant reductions in chattering and improved trajectory tracking performance even under parameter uncertainties [6].

The remainder of the paper is structured as follows: Section 2 reviews the dynamic model of robotic manipulators and foundational concepts of SMC and ISMC. Section 3 presents the proposed ISMC design. Section 4 discusses simulation and experimental results, and section 5 concludes with future research directions.

2. FRAMEWORK ROBOT DYNAMICS AND SMC-BASED CONTROL PRINCIPLES

In designing an advanced sliding mode control (SMC) scheme for robotic manipulators, it is important to recognize that these systems can generally be represented as second-order nonlinear dynamic systems. This characteristic makes them particularly suitable for control techniques that can handle nonlinearities and model uncertainties effectively. In this section, a sequential hand-held robot motion control system described by the following dynamic equation [34]:

$$\boldsymbol{M}(q)\ddot{\boldsymbol{q}} + \boldsymbol{N}(q,\dot{q})\dot{\boldsymbol{q}} + \boldsymbol{G}(q) + \boldsymbol{D}(t) = \boldsymbol{F}(t) \tag{1}$$

where the matrix (**M, N**)$\in R^{nxn}$ are the feature of the inertial, centrifugal and Coriolis force matrix, (**G, D, F**)$\in R^{nx1}$ are the feature of the gravity, disturbance and control signal vectors. **q** = $[q_1, \ldots q_n]^T \in R^{nx1}$ is a variable joint vector. Each joint corresponds to a degree of freedom.

The model (1) has the following properties:

a. **M***(q)*, $\boldsymbol{N}(q,\dot{q})\dot{q}$ are define positive determinants, at the same time ($\dot{\boldsymbol{M}}(q)$ – $2\boldsymbol{N}(q,\dot{q})\dot{q}$) is the symmetric rotation matrix, i.e., $\boldsymbol{x}^T\big(\boldsymbol{M}(q) - \boldsymbol{N}(q,\dot{q})\big)\boldsymbol{x} = 0$, with $\boldsymbol{x} \in R^{nx1}$.
b. The elements of **M***(q)*, $\boldsymbol{N}(q,\dot{q})$ are unknown so they have above and below limit.
c. Disturbance **D***(t)* is not measured, so it has above limit, $D^+ = sup_\infty \|D(t)\|$.

The control goal is to design **F**(t) the system tracks a desired trajectory q_d, minimizing the tracking error $q_e = q - q_d$ is a smallest.

Since **M***(q)*, $\boldsymbol{N}(q,\dot{q})$ cannot be accurately determined, we use the model of estimation through the dynamic description. However, we assume that the model deviation does not exceed the estimated value. With this assumption, we do not use the model state observer. Therefore, the calculation results will be inferred for the system to add parameter variability. From the defining parameters of the trajectory, note that the actual position **q** and the deviation qe are measurable, we have:

$$\dot{\boldsymbol{q}} = \dot{\boldsymbol{q}}_e + \dot{\boldsymbol{q}}_d; \ddot{\boldsymbol{q}} = \ddot{\boldsymbol{q}}_e + \ddot{\boldsymbol{q}}_d \tag{2}$$

where velocity and acceleration are to be limited. Actually, the velocity is naturally limited by the motor rated voltage, and the acceleration depends on the limit of the current at nominal value. Replace (2) into (1) will receive:

$$\boldsymbol{M}(q)\ddot{\boldsymbol{q}}_e + \boldsymbol{N}(q,q)\dot{\boldsymbol{q}}_e + \boldsymbol{G}(q) + \boldsymbol{D}(t) + \boldsymbol{Q}_d(q,q_d) = \boldsymbol{F}(t) \tag{3}$$

In that formula (3): $\boldsymbol{Q}_d(q,q_d) = \boldsymbol{M}(q)\ddot{\boldsymbol{q}}_d + \boldsymbol{N}(q,\dot{q})\dot{\boldsymbol{q}}_d \in R^{nxn}$ is the matrix is defined immediately, so it is considered as known quantity.

Choose a sliding surface [1,2]:

$$\begin{aligned}&\boldsymbol{S}_0 = \dot{\boldsymbol{q}}_e + \boldsymbol{\lambda}\boldsymbol{q}_e = 0; \boldsymbol{S}_0 \in R^{nx1},\\ &\boldsymbol{\lambda} = diag(\lambda_i), \lambda_i = const > 0, i = 1..n\end{aligned} \tag{4}$$

For the slider mode to exist, the control signal F must be selected to the satisfy sliding condition [2]:

$$\boldsymbol{S}^T\boldsymbol{M}(q)\dot{\boldsymbol{S}} < -\eta, \eta > 0 \tag{5}$$

With outside of surface. In that, $\boldsymbol{S} = \dot{\boldsymbol{q}}_e + \boldsymbol{\lambda}\boldsymbol{q}_e, \boldsymbol{S} \in R^{nx1}$is a state vector of system, λ is a diagonal matrix that contains constant elements. Combine (2), (3) and (4).

$$\boldsymbol{M}(q)\dot{\boldsymbol{S}} = \boldsymbol{F} - \boldsymbol{N}(q,\dot{q})\dot{q}_e - \boldsymbol{Q}_d(q,q_d) - \boldsymbol{G}(q) - \boldsymbol{D}(t) + \boldsymbol{M}\boldsymbol{\lambda}\dot{\boldsymbol{q}}_e = \boldsymbol{F} - \boldsymbol{f}_q \tag{6}$$

Here, $\boldsymbol{f}_q = \boldsymbol{N}(q)\dot{\boldsymbol{q}}_e + \boldsymbol{Q}_d(q,q_d) + \boldsymbol{G}(q) + \boldsymbol{D}(t) - \boldsymbol{M}\boldsymbol{\lambda}\dot{\boldsymbol{q}}_e$ is also a computable regression if the noise is measured.

Replace (6) into (5), the sliding condition becomes (7).

$$\boldsymbol{S}^T(\boldsymbol{F} - \boldsymbol{f}_q) < -\eta \tag{7}$$

If we choice:

$$\boldsymbol{F} = \boldsymbol{f}_q - \boldsymbol{K}\, sgn(\boldsymbol{S}) \tag{8}$$

With **K** = *diag(k)* $\in R^{nxn}$ is a diagonal matrix that contains positive elements, denote auxiliary vector $\mathbf{J}=[1,...,1]^T \in R^{nx1}$, condition (7) will be satisfied. However, the difficulty here is how to determine $\mathbf{f}_q$, because the noise is not accurately measured, as the matrix coefficients **M, N**, and **G** are estimated values. So if you call $\boldsymbol{\sigma}_D = diag(sup_\infty|D(t)|) \in R^{nxn}$ as the diagonal matrix contains the upper bound of the noise, we can choose the control law:

$$\boldsymbol{F} = \boldsymbol{Q}_d(q,q_d) + \boldsymbol{G}(q) - \boldsymbol{M}\boldsymbol{\lambda}\dot{\boldsymbol{q}}_e - \boldsymbol{N}(q)\boldsymbol{\lambda}\boldsymbol{q}_e - (\boldsymbol{\sigma}_D + \boldsymbol{\sigma}_H + \boldsymbol{K})\, sgn(\boldsymbol{S}) \tag{9}$$

Denote:

$$\boldsymbol{\sigma}_M = \Delta\boldsymbol{M}nxn_N nxn_{max_{max}} \qquad \boldsymbol{\sigma}_G = \Delta\boldsymbol{G}nx1_H\, sup_\infty|\Delta\boldsymbol{H}|^{nxn}{}_{max}$$

are the upper bounds of the biased elements in the model parameter matrix. Then the desired model will be formed:

$$\begin{aligned}\boldsymbol{F}(t) &= (\boldsymbol{M} + \Delta\boldsymbol{M})\ddot{\boldsymbol{q}}_e + (\boldsymbol{N} + \Delta\boldsymbol{N})\dot{\boldsymbol{q}}_e + (\boldsymbol{G} + \Delta\boldsymbol{G}) + \boldsymbol{D}(t) + \boldsymbol{Q}_d(q,q_d)\\ &= \boldsymbol{M}(q)\ddot{\boldsymbol{q}}_e + \boldsymbol{N}(q,q)\dot{\boldsymbol{q}}_e + \boldsymbol{G}(q) + \boldsymbol{D}(t) + \boldsymbol{Q}_d(q,q_d) + \Delta\boldsymbol{H}\end{aligned} \tag{10}$$

With $\Delta\boldsymbol{H} = \Delta\boldsymbol{M}(q)\ddot{\boldsymbol{q}}_e + \Delta\boldsymbol{N}(q,q)\dot{\boldsymbol{q}}_e + \Delta\boldsymbol{G}(q)$ called false vector model balance. Can see immediately:

$$\Delta\boldsymbol{H} = \Delta\boldsymbol{M}(q)\ddot{\boldsymbol{q}}_e + \Delta\boldsymbol{N}(q,q)\dot{\boldsymbol{q}}_e + \Delta\boldsymbol{G}(q) \le \boldsymbol{\sigma}_M|\ddot{\boldsymbol{q}}_e| + \boldsymbol{\sigma}_N|\dot{\boldsymbol{q}}_e| + \boldsymbol{\sigma}_G \le \boldsymbol{\sigma}_H\boldsymbol{J} \tag{11}$$

Proof: Choose Lyapunov candidate:

$$\boldsymbol{V} = \frac{1}{2}\boldsymbol{S}^T\boldsymbol{M}(q)\boldsymbol{S} \tag{12}$$

To do derivation of (12) we have:

$$\dot{\boldsymbol{V}} = \boldsymbol{S}^T\boldsymbol{M}\dot{\boldsymbol{S}} + \tfrac{1}{2}\boldsymbol{S}^T\dot{\boldsymbol{M}}\boldsymbol{S} \tag{13}$$

Combine (6), (9), (10) into (13) we will have:

$$\begin{aligned}\dot{\boldsymbol{V}} &= \boldsymbol{S}^T(\boldsymbol{F} + \boldsymbol{M}(q)\boldsymbol{\lambda}\dot{\boldsymbol{q}}_e - \boldsymbol{N}(q,\dot{q})\dot{\boldsymbol{q}}_e - \boldsymbol{G}(q) - \boldsymbol{D}(t) - \boldsymbol{Q}_d(q,q_d) - \Delta\boldsymbol{H}) + \frac{1}{2}\boldsymbol{S}^T\dot{\boldsymbol{M}}\boldsymbol{S}\\ &= \boldsymbol{S}^T(-\boldsymbol{N}(q,\dot{q})\dot{\boldsymbol{q}}_e - \boldsymbol{N}(q,\dot{q})\boldsymbol{\lambda}\boldsymbol{q}_e - \boldsymbol{D}(t) - \Delta\boldsymbol{H} - (\boldsymbol{\sigma}_D + \boldsymbol{\sigma}_H + \boldsymbol{K})\,sgn(\boldsymbol{S})) + \frac{1}{2}\boldsymbol{S}^T\dot{\boldsymbol{M}}\boldsymbol{S}\\ &= \boldsymbol{S}^T(-\boldsymbol{N}(q,\dot{q})\boldsymbol{S} - \boldsymbol{D}(t) - \Delta\boldsymbol{H} - (\boldsymbol{\sigma}_D + \boldsymbol{\sigma}_H + \boldsymbol{K})\,sgn(\boldsymbol{S})) + \frac{1}{2}\boldsymbol{S}^T\dot{\boldsymbol{M}}\boldsymbol{S}\\ &= \boldsymbol{S}^T(\boldsymbol{D} - \Delta\boldsymbol{H} - (\boldsymbol{\sigma}_D + \boldsymbol{\sigma}_H + \boldsymbol{K})\,sgn(\boldsymbol{S})) + 0.5\boldsymbol{S}^T(\dot{\boldsymbol{M}} - 2\boldsymbol{N})\boldsymbol{S} < 0\end{aligned} \tag{14}$$

If we denote $\boldsymbol{K}_s = (\boldsymbol{\sigma}_D + \boldsymbol{\sigma}_H + \boldsymbol{K})\boldsymbol{J} = \boldsymbol{K}_0 + \boldsymbol{K}$, K_0 will be pre-selected based on experience and model experience. With the selected control signal, the system will stabilize and the slider mode will exist. From SMC properties, we can see that while working point runs away balance point, then system needs big value of K to hit to balance zone, and if system has done inside balance zone, we will reduce K to do nots make big change of motion. We have illustration as Figure 1. In that, maximize value of K has limited to do assurance of stabilization.

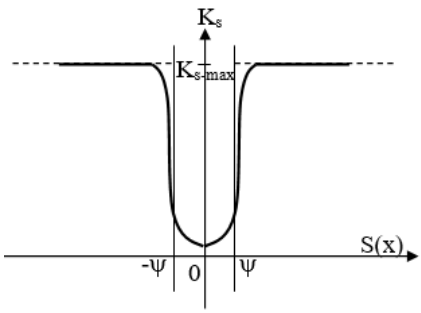

Figure 1. Description of change of K in the SMC

There are some considerations in (14), since $\Delta\mathbf{D}$ and $\Delta\mathbf{H}$ are infinite norms of noise and model distortion, so the first component in brackets in the left side of (14) always goes upside to **S**, so both the matrix multiplication will always be negative, the second component on the left side is zero because of the property of the parameter. Thus, the mode always exists with the control signal (9). Control signals (9) can be separated into two components:

$$\boldsymbol{F} = \boldsymbol{Q}_d(q,q_d) + \boldsymbol{G}(q) - \boldsymbol{M}\boldsymbol{\lambda}\dot{\boldsymbol{q}}_e - \boldsymbol{N}(q)\boldsymbol{\lambda}\boldsymbol{q}_e - (\boldsymbol{\sigma}_D + \boldsymbol{\sigma}_H + \boldsymbol{K})\,sgn(\boldsymbol{S}) = \boldsymbol{F}_{eq} + \boldsymbol{F}_d$$

In that

$$\boldsymbol{F}_{eq} = \boldsymbol{Q}_d(q,q_d) + \boldsymbol{G}(q) - \boldsymbol{M}\boldsymbol{\lambda}\dot{\boldsymbol{q}}_e - \boldsymbol{N}(q)\boldsymbol{\lambda}\boldsymbol{q}_e,$$
$$\boldsymbol{F}_d = -(\boldsymbol{\sigma}_D + \boldsymbol{\sigma}_H + \boldsymbol{K})\,sgn(\boldsymbol{S})$$

The signal is called the continuous equivalent and interrupt. The F_{eq} component to keep the system stable and slip-free, while the F_d component to keep the system stable with noise and parameter modification, if in the absence of interference and constant parameters, F_d can reduced to zero. The symbol $[S] = [|S_1|, |S_2|, \ldots, |S_n|]^T$.

3. PROPOSED ADAPTIVE ISMC APPROACH

Based on the dynamic model and sliding mode control concepts introduced in section 2, this section presents the proposed ISMC strategy with adaptive gain tuning. The primary objective of this approach is to enhance control performance by addressing two key challenges in traditional SMC: excessive chattering and limited adaptability under model uncertainties and external disturbances.

To achieve this, our method integrates two mechanisms: i) an adaptive gain law using an exponential integral function to dynamically regulate the switching gain K, and ii) a boundary layer method to smoothen the control signal near the sliding surface. The core contribution of this work lies in the development of an observer-free ISMC algorithm that enables real-time gain adjustment without requiring precise system models or external state estimators. From a control perspective, the proposed method applies independent sliding surfaces for each joint degree of freedom, allowing joint-level tuning of the control effort. This design improves motion stability by reducing the amplitude of the discontinuous control component E_d, thereby suppressing vibration in the joint trajectories.

The remainder of this section provides the theoretical formulation of the proposed adaptive gain algorithm, including its Lyapunov-based stability proof and design parameters.

Theory: K_s adaptive method to reduce vibration by ISMC algorithm.

Statement: For system (1), use sliding surface (4) with control rule (9), if K_s contains K_{si} elements that follow:

$$K_{si} = (1 + sgn(|q_{ei}| - \delta_i))e^{|q_{ei}|} + K_{0i} + e^{\int_{t_1}^{t_2}(|S_i| - \psi_i)dt} \quad i=1, \ldots, n \tag{15}$$

Then the trajectory of the system (1) will follow the desired trajectory, with the static deviation reaching zero in the range $|S_i| < \psi_i$ and establish error $q_{ei} < \delta_i$. In that ψ and δ are two vectors containing arbitrarily small positive elements, depending on the permissive requirement of the systematic discrepancy (1). Then the K_s vector is denoted as: $K_s = (1 + sgn(|q_e| - \delta))e^{|q_e|} + K_0 + e^{\int_{t_1}^{t_2}(|S| - \psi)dt}$.

Proof: If we choose $K_{0i} > \eta_i$, $i=1..n$ will ensure the sliding condition exists. In addition, the vector components in the right-hand side of (15) show:

$$(1 + sgn(|q_{ei}| - \delta_i))e^{|q_{ei}|} = \begin{cases} 0 khi |q_{ei}| < \delta_i \\ 2e^{|q_{ei}|} > 0 khi |q_{ei}| > \delta_i \end{cases} \quad i=1, \ldots, n \tag{16}$$

$$e^{\int_{t_1}^{t_2}(|S| - \psi_i)dt} > 0 \forall S_i \quad i=1, \ldots, n \tag{17}$$

Thus, K_{si} in (15) will always be positive so the system is always stable on the sliding surface. Demonstration of the statement confirms two problems: static chattering amplitude and deviation decrease if the kinetic energy and potential energy of the orbital deviation decreases using the adaptive algorithm (15). Using the Lyapunov function [16]:

$$V = \frac{1}{2}\boldsymbol{q}_e^T \boldsymbol{q}_e + \frac{1}{2}\dot{\boldsymbol{q}}_e^T \dot{\boldsymbol{q}}_e \tag{18}$$

Derivate a V candidate function is:

$$\dot{V} = \dot{\boldsymbol{q}}_e^T \boldsymbol{q}_e + \dot{\boldsymbol{q}}_e^T \ddot{\boldsymbol{q}}_e = \dot{\boldsymbol{q}}_e^T (\boldsymbol{q}_e - \boldsymbol{\lambda}\dot{\boldsymbol{q}}_e - [diag(sgn(\boldsymbol{S}))]\boldsymbol{K}_s) \tag{19}$$

If exist a diagonal matrix $\boldsymbol{g} \in R^{nxn}$ contains positive elements:

$$\begin{aligned} &(\boldsymbol{q}_e - \boldsymbol{\lambda}\dot{\boldsymbol{q}}_e - [diag(sgn(\boldsymbol{S}))]\boldsymbol{K}_s) = -\boldsymbol{g}\dot{\boldsymbol{q}}_e \\ &\Rightarrow \boldsymbol{q}_e + (\boldsymbol{g} - \boldsymbol{\lambda})\dot{\boldsymbol{q}}_e = [diag(sgn(\boldsymbol{S}))]\boldsymbol{K}_s \end{aligned} \tag{20}$$

Then derivation of V will a negative value. Reply (15) into (20) we have:

$$\boldsymbol{q}_e + (\boldsymbol{g} - \boldsymbol{\lambda})\dot{\boldsymbol{q}}_e = [diag(sgn(\boldsymbol{S}))]\left[(1 + sgn(|\boldsymbol{q}_e| - \boldsymbol{\delta}))e^{|\boldsymbol{q}_e|} + \boldsymbol{K}_0 + e^{\int_{t_1}^{t_2}(|\boldsymbol{S}| - \boldsymbol{\psi})dt}\right] \tag{21}$$

From (16), (17) we only proof property of theory in the domain $|S_i|<\psi_i$, $i=1, \ldots, n$. Because is defined with λ = constant, so the error of trajectory q_i will be decision [2]:

$$q_{ei} = \int_0^T e^{-\lambda_i(T-t)} S_i dt \le \psi_i \int_0^T e^{-\lambda_i(T-t)} dt = \psi_i \lambda_i^{-1}\left(1 - e^{-\lambda_i T}\right) \le \psi_i \lambda_i^{-1} \quad i=1, \ldots, n \tag{22}$$

In general, in choice $\delta = \lambda^{-1}\psi$ then while **S** moves in the sliding layer **ψ**, then $\mathbf{q}_e$ also moves in the error layer of the **δ**:

+ While $S_i>0$ then $(-\lambda_i q_{ei} < \dot{q}_{ei})$, $i=1, \ldots, n$. From (21) we could write:

$$\boldsymbol{q}_e + (\boldsymbol{g} - \boldsymbol{\lambda})\dot{\boldsymbol{q}}_e = (\boldsymbol{I} - \boldsymbol{g\lambda} + \boldsymbol{\lambda}^2)\boldsymbol{q}_e + \boldsymbol{z} \tag{24}$$

With value $z=[z_1, ..., z_n]^T$, $z_i>0$, $i=1, ..., n$. So $q_{ei} \leq \delta_i$ then we could design a parameter g to:

$$(\boldsymbol{I} - \boldsymbol{g\lambda} + \boldsymbol{\lambda}^2) = \boldsymbol{\alpha Q}_\delta \tag{25}$$

With $\boldsymbol{Q}_\delta = diag[\delta_i], \delta_i > 0, i = 1..n$,
$\boldsymbol{\alpha} = diag[\alpha_i] \in R^{nxn}, \alpha_i \geq 0$. From here we have:

$$\boldsymbol{g} = (\boldsymbol{I} + \boldsymbol{\lambda}^2 - \boldsymbol{\alpha Q}_\delta)\boldsymbol{\lambda}^{-1} \tag{26}$$

According to the hypothesis of **g**, the left side of (26) is always positive, so that leads to:

$$\begin{aligned}&(\boldsymbol{I} + \boldsymbol{\lambda}^2 - \boldsymbol{\alpha Q}_\delta) = \boldsymbol{\Gamma},\\ &\boldsymbol{\Gamma} = \boldsymbol{diag}[\boldsymbol{\gamma}_i] \in \boldsymbol{R}^{nxn}, \boldsymbol{\gamma}_i > \boldsymbol{0}\end{aligned} \tag{27}$$

$$\Rightarrow \boldsymbol{\lambda}^2 = \boldsymbol{\alpha Q}_\delta + \boldsymbol{\Gamma} - \boldsymbol{I} \tag{28}$$

If we choice **α**, **Γ** is well then condition (28) has completely satisfied, then it will be determined that **g** contains the elements of (26). So condition (20) will give:

$$\dot{\boldsymbol{V}} = \dot{\boldsymbol{q}}_e^T(\boldsymbol{q}_e - \boldsymbol{\lambda}\dot{\boldsymbol{q}}_e - [\boldsymbol{diag}(\boldsymbol{sgn}(\boldsymbol{S}))]\boldsymbol{K}_s) = -\dot{\boldsymbol{q}}_e^T\boldsymbol{g}\dot{\boldsymbol{q}}_e < \boldsymbol{0} \tag{29}$$

+ When $S_i<0$, (21) becomes:

$$\boldsymbol{q}_e - (\boldsymbol{g} - \boldsymbol{\lambda})\dot{\boldsymbol{q}}_e = \boldsymbol{q}_e - (\boldsymbol{g} - \boldsymbol{\lambda})\boldsymbol{\lambda q}_e - \boldsymbol{z} = (\boldsymbol{I} - \boldsymbol{g\lambda} + \boldsymbol{\lambda}^2)\boldsymbol{q}_e - \boldsymbol{z} \tag{30}$$

So, if we choice $\boldsymbol{g}$ by:

$$\boldsymbol{g} = (\boldsymbol{I} + \boldsymbol{\lambda}^2 + \boldsymbol{\alpha Q}_\delta)\boldsymbol{\lambda}^{-1} \text{with } \alpha_i < \frac{z_i}{\delta_i^2}, i = 1..n \tag{31}$$

Then the expression (20) will be satisfied and the matrix **g** will contain positive elements. The combinations (26), (28) and (31) will be found in the case of **S**, always finding the matrix g to condition (19) for the result:

$$\dot{\boldsymbol{V}} = \dot{\boldsymbol{q}}_e^T(\boldsymbol{q}_e - \boldsymbol{\lambda}\dot{\boldsymbol{q}}_e - [diag(sgn(\boldsymbol{S}))]\boldsymbol{K}_s) = -\dot{\boldsymbol{q}}_e^T\boldsymbol{g}\dot{\boldsymbol{q}}_e < 0 \tag{32}$$

Therefore, we have: $lim_{t\to\infty}(\boldsymbol{q}_e^T\boldsymbol{q}_e) < lim_{t\to\infty}(V) = 0$.
Equations (29) and (32) assert that the function V always decreases the potential energy and kinetic energy, so the system will reduce vibration and static deviation to zero [34]. If **S** contains positive and negative elements, then we divide **S** into two vectors containing distinct positive and negative elements, and demonstrate the same as for the matrix **g**. This method has some characteristics:

a. Ensures continuous variation of Ks within the error range δ. Ks increases and decreases with the error δ and also the error when following the sliding surface, so the adaptability is better than existing methods.
b. When the error exceeds δ, Ks changes greatly to quickly find the sliding surface.
c. The integration process does not cause Ks to change sign in the near-time range.
d. The ability to resist disturbances is better than integration, and the established error can be controlled.

We do expression of Taylor exponential function integrates in the adjacent sliding surface class we have:

$$e^{\int_{t_0}^{t_1}(|S|-\psi)dt} = 1 + \int_{t_0}^{t_1}(|S| - \psi)dt + \frac{\left(\int_{t_0}^{t_1}(|S|-\psi)dt\right)^2}{2!} + \frac{\left(\int_{t_0}^{t_1}(|S|-\psi)dt\right)^3}{3!} + \ldots + R(S) \tag{33}$$

Approximate approximation of the first component, as seen with the SMAC method, the control function for the object will now be approximated:

$$u \approx u_{eq} + K_i\left(1 + \int_{t_0}^{t_1}(|S| - \psi)dt + \frac{\left(\int_{t_0}^{t_1}(|S|-\psi)dt\right)^2}{2!} + \frac{\left(\int_{t_0}^{t_1}(|S|-\psi)dt\right)^3}{3!}\right)(sgn(S)) \tag{34}$$

In the sliding surface, the integral decreases, so if the expansion factor is large, the integral value becomes smaller. Looking at (34), the controller behaves as a proportional-integral phase, an infinite-integral form that satisfies, but extends over time. Thus, according to control theory, PI-compensated structures are suitable for medium and large inertia objects such as electromechanical devices and robots. The advantage of this method is that it cannot be processed. Parametric deflection parameter driven by the exponent misalignment ratio at the beginning of the parameter fitting law, which the previous methods do not yet do.

4. EXPERIMENT AND DISCUSSION

This section presents the experimental validation and result analysis of the proposed ISMC strategy. To evaluate the effectiveness and practicality of the proposed controller, extensive experiments were conducted on robotic manipulator systems. The tests were designed to assess the performance of the ISMC algorithm in terms of trajectory tracking accuracy, convergence speed, and robustness against external disturbances and uncertainties. The following subsections detail the algorithm implementation and validation, followed by a thorough analysis of the experimental results.

4.1. Experiment setting

The contributions distinguish the proposed ISMC algorithm as a practical and effective solution for advanced robotic control applications where both robust performance and mechanical longevity are paramount. The simulation results for the two-link robot manipulator (Figure 2) were carried out to verify the proposed ISMC method. The robot's physical parameters include: link masses $m_1 = m_2 = 2$, kg, link lengths $l_1 = l_2 = 0.3$, m, and moments of inertia $J_1 = J_2 = 0.02$, kg · m^2, with uniformly distributed masses.

To evaluate the ISMC approach, the trajectory was set as $q_{d1} = 10\cos(t)$ and $q_{d2} = 10\sin(t)$. In the simulation, an initial error of 1 was used to test the system's response to a variable gain Ks in the ISMC algorithm, while a fixed gain $K_s = 50$ was used for comparison.

4.2. Experiment results

Figure 3 illustrates the process of convergence to the sliding surface, and Figure 4 show the results of the simulation. The results indicate that the robot system exhibits high stability despite variations in noise and parameters. The system's parameter matrices also vary significantly. Figure 4 confirms that adjusting the ISMC gain Ks significantly reduces vibration amplitude compared to a traditional PID controller. In the region of permissible trajectory deviation δ, the system operates with minimal gain K, and the inclusion of an exponential difference term in the trajectory ensures not only stability under bias disturbances but also improved deviation control in low-noise scenarios. Experiments were conducted using a 3-DoF robotic manipulator depicted in Figure 5. Figures 6 and 7 illustrate the trajectory tracking error of the three joints of the robotic manipulator under different operating conditions.

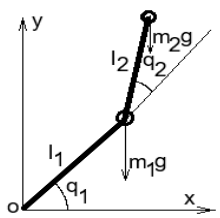

Figure 2. Robot arm 2DoF

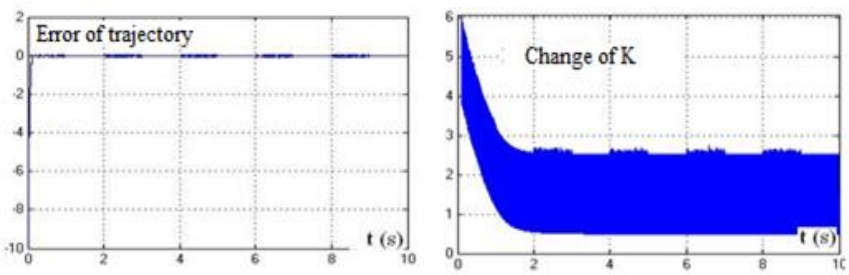

Figure 3. The error change K_s by time of ISMC method

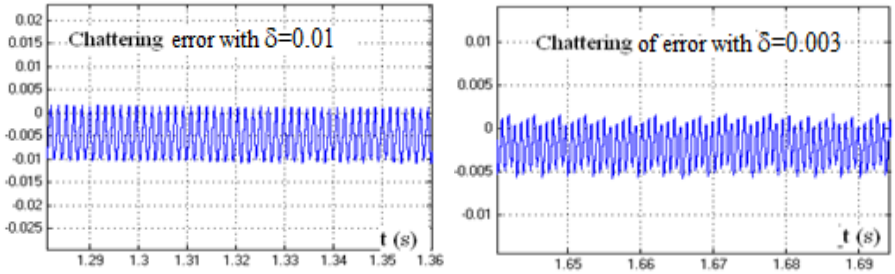

Figure 4. Simulation error with any value of δ

Figure 5. The experiment model of robot 3D

4.3. Discussion

Figure 3 illustrates the time response of trajectory tracking error and the evolution of the adaptive gain K_s in the proposed ISMC framework. As shown in the left subfigure, the trajectory error converges rapidly to zero and remains bounded, demonstrating the effectiveness of the ISMC controller in ensuring stable tracking performance. The right subfigure shows that the gain K_s starts at a relatively high value to ensure strong corrective action during the initial transient phase. Over time, as the system approaches the sliding surface and the tracking error decreases, K_s is gradually reduced according to the exponential adaptation law. This behavior effectively avoids excessive control effort and contributes to chattering suppression.

Figure 4 compares the chattering behavior under two different values of the design parameter δ, which regulates the exponential decay rate of K_s. The left plot corresponds to a larger value (δ=0.01), where chattering oscillations in the error are more pronounced. In contrast, the right plot, with δ=0.003, shows significantly reduced oscillation amplitude. This comparison highlights that smaller δ values result in a slower decrease in gain K_s, allowing more gradual adaptation and better damping of the control signal. However, excessively small δ may reduce responsiveness. Thus, a proper selection of δ balances the trade-off between fast convergence and chattering attenuation. These results confirm that the proposed ISMC controller not only achieves robust and accurate trajectory tracking but also adaptively modulates control gains to suppress chattering, enhancing both performance and practical applicability in robotic systems.

Additionally, the experiments with robot 3DoF in the no-load case in Figure 6, the tracking errors for joints 1, 2, and 3 exhibit small initial deviations that rapidly converge to zero. Joint 2 shows the largest initial deviation of approximately 1.2 radians, which stabilizes after about 4 seconds. In contrast, joint 1 and joint 3 display smaller deviations and reach zero error even faster. When a 1 kg load is applied in Figure 7, the initial tracking errors increase, with joint 2 reaching up to 1.5 radians, joint 1 at about 1.2 radians, and joint 3 around 0.8 radians. This increase reflects the additional inertia and external disturbances caused by the load. However, despite these challenges, the tracking errors of all joints still converge to zero within approximately 8 seconds. The slightly longer convergence time and increased transient errors under load highlight the system's dynamic response to external disturbances. Hence, these results confirm that the proposed ISMC controller effectively adapts to both no-load and loaded conditions, ensuring robust trajectory tracking and significant suppression of chattering, even in the presence of parameter uncertainties and external disturbances.

These experiments demonstrated that vibration was minimal and did not affect the trajectory, even when the input disturbance changed continuously from zero to maximum. Although the transition phase lasted up to 2 seconds, it was acceptable, and the system maintained the desired static accuracy. The experiments confirm that the proposed ISMC algorithm effectively suppresses the chattering phenomenon in

SMC, while maintaining high trajectory tracking performance. Notably, this approach is not only applicable to robot manipulators but can also be extended to other moving systems governed by Lagrangian dynamics.

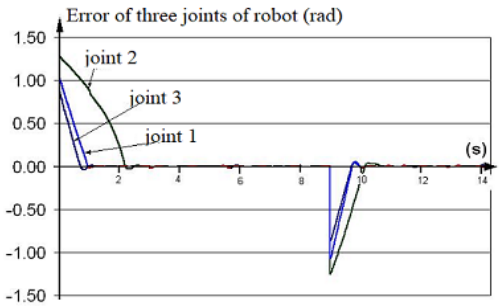

Figure 6. The error of three joints of robot with no load

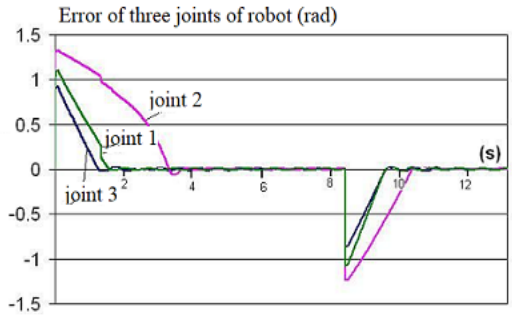

Figure 7. The error of three joints of robot with load 1 kg

5. CONCLUSION

In this work, an integral sliding mode control strategy with an adaptive exponential gain law (ISMC) was proposed to overcome the chattering issue in conventional SMC schemes for robotic manipulators. The method adaptively tunes the switching gain $\boldsymbol{K}$ in real-time based on the integral of the sliding surface, without requiring observer-based estimation or model restructuring. Lyapunov-based stability analysis proved the global stability of the closed-loop system. Extensive simulation results on robotic manipulators with 2-DOF and 3-DOF validated the proposed method's effectiveness in ensuring accurate trajectory tracking and significantly reducing control effort fluctuations. The main advantages of the ISMC approach include simplified implementation, strong robustness to disturbances, and improved smoothness of control actions. These qualities make it highly suitable for practical deployment in industrial robotic systems.

AUTHOR CONTRIBUTIONS STATEMENT

This journal uses the Contributor Roles Taxonomy (CRediT) to recognize individual author contributions, reduce authorship disputes, and facilitate collaboration.

Name of Author	C	M	So	Va	Fo	I	R	D	O	E	Vi	Su	P	Fu
Mai Hoang Nguyen	✓	✓	✓	✓	✓	✓	✓	✓	✓	✓	✓	✓	✓	
Truc Thi Kim Nguyen		✓				✓		✓		✓	✓	✓		

C : **C**onceptualization
M : **M**ethodology
So : **So**ftware
Va : **Va**lidation
Fo : **Fo**rmal analysis
I : **I**nvestigation
R : **R**esources
D : **D**ata Curation
O : Writing - **O**riginal Draft
E : Writing - Review & **E**diting
Vi : **Vi**sualization
Su : **Su**pervision
P : **P**roject administration
Fu : **Fu**nding acquisition

CONFLICT OF INTEREST STATEMENT

The authors declare that they have no known financial, personal, or professional conflicts of interest that could have influenced the research and findings reported in this paper. No competing interests exist.

DATA AVAILABILITY

The data that support the findings of this study are available from the corresponding author, M.H.N., upon reasonable request.

REFERENCES

[1] S. H. Han, M. S. Tran, and D. T. Tran, "Adaptive sliding mode control for a robotic manipulator with unknown friction and unknown control direction," *Applied Sciences (Switzerland)*, vol. 11, no. 9, 2021, doi: 10.3390/app11093919.

[2] C. Jing, H. Zhang, Y. Liu, and J. Zhang, "Adaptive super-twisting sliding mode control for robot manipulators with input saturation," *Sensors*, vol. 24, no. 9, 2024, doi: 10.3390/s24092783.

[3] Y. Shtessel, C. Edwards, L. Fridman, and A. Levant, "Sliding mode control and observation," *Sliding Mode Control and Observation*, pp. 1–356, 2014, doi: 10.1007/978-0-8176-4893-0.

[4] K. D. Young and S. V. Drakunov, "Sliding mode control with chattering reduction," in *Proceedings of the American Control Conference*, 1992, vol. 2, pp. 1291–1294, doi: 10.23919/acc.1992.4792307.

[5] F. F. M. El-Sousy, M. M. Amin, and O. A. Mohammed, "Robust adaptive neural network tracking control with optimized super-twisting sliding-mode technique for induction motor drive system," *IEEE Transactions on Industry Applications*, vol. 58, no. 3, pp. 4134–4157, 2022, doi: 10.1109/TIA.2022.3160136.

[6] M. A. Ranjbar, "Fast finite-time sliding mode control for chattering-free trajectory tracking of robotic manipulators," *Electrical Engineering and Systems Science*, 2025.

[7] M. Gao, L. Ding, and X. Jin, "ELM-based adaptive faster fixed-time control of robotic manipulator systems," *IEEE Transactions on Neural Networks and Learning Systems*, vol. 34, no. 8, pp. 4646–4658, 2023, doi: 10.1109/TNNLS.2021.3116958.

[8] Y. Liang, D. Zhang, G. Li, and T. Wu, "Adaptive chattering-free pid sliding mode control for tracking problem of uncertain dynamical systems," *Electronics (Switzerland)*, vol. 11, no. 21, 2022, doi: 10.3390/electronics11213499.

[9] R. Svečko, D. Gleich, and A. Sarjaš, "The effective chattering suppression technique with adaptive super-twisted sliding mode controller based on the quasi-barrier function; an experimentation setup," *Applied Sciences (Switzerland)*, vol. 10, no. 2, 2020, doi: 10.3390/app10020595.

[10] X. Lin, F. Du, J. Song, C. Yin, Y. Zhang, and Y. Li, "Robust continuous sliding mode torque tracking control for compliant actuators with prescribed performance," *International Journal of Control, Automation and Systems*, vol. 23, no. 3, pp. 882–895, 2025, doi: 10.1007/s12555-024-0470-7.

[11] J. Liu, Y. Cui, H. Wang, Y. Tian, and X. Zhou, "Rigid spacecraft attitude control based on finite-time non-singular sliding mode and extended state disturbance observer with input hysteresis," *International Journal of Robust and Nonlinear Control*, vol. 35, no. 10, pp. 4187–4200, 2025, doi: 10.1002/rnc.7896.

[12] M. Ramesh, A. K. Yadav, P. K. Pathak, and C. H. H. Basha, "A novel fuzzy assisted sliding mode control approach for frequency regulation of wind-supported autonomous microgrid," *Scientific Reports*, vol. 14, no. 1, 2024, doi: 10.1038/s41598-024-83202-z.

[13] T. Zou, H. Wu, W. Sun, and Z. Zhao, "Adaptive neural network sliding mode control of a nonlinear two-degrees-of-freedom helicopter system," *Asian Journal of Control*, vol. 25, no. 3, pp. 2085–2094, 2023, doi: 10.1002/asjc.2862.

[14] M. Liu, Q. Tang, Y. Li, C. Liu, and M. Yu, "A chattering-suppression sliding mode controller for an underwater manipulator using time delay estimation," *Journal of Marine Science and Engineering*, vol. 11, no. 9, 2023, doi: 10.3390/jmse11091742.

[15] J. Wang, P. Zhu, B. He, G. Deng, C. Zhang, and X. Huang, "An adaptive neural sliding mode control with ESO for uncertain nonlinear systems," *International Journal of Control, Automation and Systems*, vol. 19, no. 2, pp. 687–697, 2021, doi: 10.1007/s12555-019-0972-x.

[16] P. Yue, B. Xu, and M. Zhang, "An improve nonlinear robust control approach for robotic manipulators with PSO-based global optimization strategy," *Scientific Reports*, vol. 14, no. 1, 2024, doi: 10.1038/s41598-024-72156-x.

[17] M. Raoufi, H. Habibi, A. Yazdani, and H. Wang, "Robust prescribed trajectory tracking control of a robot manipulator using adaptive finite-time sliding mode and extreme learning machine method," *Robotics*, vol. 11, no. 5, 2022, doi: 10.3390/robotics11050111.

[18] H. V. A. Truong, D. T. Tran, and K. K. Ahn, "A neural network based sliding mode control for tracking performance with parameters variation of a 3-DOF manipulator," *Applied Sciences (Switzerland)*, vol. 9, no. 10, 2019, doi: 10.3390/app9102023.

[19] M. The Vu *et al.*, "Robust position control of an over-actuated underwater vehicle under model uncertainties and ocean current effects using dynamic sliding mode surface and optimal allocation control," *Sensors (Switzerland)*, vol. 21, no. 3, pp. 1–25, 2021, doi: 10.3390/s21030747.

[20] C. Edwards and S. Spurgeon, "Advancement and design of robotic manipulator control structures," *Journal of Computational and Theoretical Nanoscience*, vol. 16, no. 2, pp. 123–135, 2024.

[21] Q. Meng, H. Yang, and B. Jiang, "Second-order sliding-mode on SO(3) and fault-tolerant spacecraft attitude control," *Automatica*, vol. 149, p. 110814, Mar. 2023, doi: 10.1016/j.automatica.2022.110814.

[22] M. Roohi, S. Mirzajani, A. R. Haghighi, and A. Basse-O'Connor, "Robust design of two-level non-integer SMC based on deep soft actor-critic for synchronization of chaotic fractional order memristive neural networks," *Fractal and Fractional*, vol. 8, no. 9, 2024, doi: 10.3390/fractalfract8090548.

[23] J. Zhao *et al.*, "Observer-based discrete-time cascaded control for lateral stabilization of steer-by-wire vehicles with uncertainties and disturbances," *IEEE Transactions on Circuits and Systems I: Regular Papers*, vol. 70, no. 8, pp. 3347–3358, 2023, doi: 10.1109/TCSI.2023.3276945.

[24] M. Sharifi, S. Tripathi, Y. Chen, Q. Zhang, and M. Tavakoli, "Reinforcement learning methods for assistive and rehabilitation robotic systems: A survey," *IEEE Transactions on Systems, Man, and Cybernetics: Systems*, vol. 55, no. 7, pp. 4534–4551, 2025, doi: 10.1109/TSMC.2025.3555598.

[25] V. H. K, "Reinforcement learning for optimization of nanorobot navigation in bloodstreams," *Nanoscale Reports*, vol. 8, no. 1, pp. 17–20, 2025, doi: 10.26524/nr.8.7.

[26] A. Laukaitis, A. Šareiko, and D. Mažeika, "Facilitating robot learning in virtual environments: A deep reinforcement learning framework," *Applied Sciences (Switzerland)*, vol. 15, no. 9, 2025, doi: 10.3390/app15095016.

[27] X. Zou, G. Yang, R. Hong, and Y. Dai, "Chattering-free terminal sliding-mode tracking control for uncertain nonlinear systems with disturbance compensation," *JVC/Journal of Vibration and Control*, vol. 30, no. 5–6, pp. 1133–1142, 2024, doi: 10.1177/10775463231157213.

[28] M. Aljamal, S. Patel, and A. Mahmood, "Comprehensive review of robotics operating system-based reinforcement learning in robotics," *Applied Sciences (Switzerland)*, vol. 15, no. 4, 2025, doi: 10.3390/app15041840.

[29] M. M. Mohammadi and A. Erfanian, "Fully adaptive terminal sliding mode control for a class of nonlinear systems with structured and unstructured uncertainties: Theory and applications," *IEEE Transactions on Industrial Electronics*, 2025, doi: 10.1109/TIE.2025.3563710.

[30] A. Razzaghian, "A fuzzy neural network-based fractional-order Lyapunov-based robust control strategy for exoskeleton robots: Application in upper-limb rehabilitation," *Mathematics and Computers in Simulation*, vol. 193, pp. 567–583, 2022, doi: 10.1016/j.matcom.2021.10.022.

[31] F. V. A. Raj and V. K. Kannan, "Particle swarm optimized deep convolutional neural Sugeno-Takagi fuzzy PID controller in permanent magnet synchronous motor," *International Journal of Fuzzy Systems*, vol. 24, no. 1, pp. 180–201, 2022, doi: 10.1007/s40815-021-01126-6.

[32] S. Abdi, M. Zakeri, and J. Beyramzad, "Intelligent chattering free controller design for MEMS gyroscopes using adaptive fuzzy-neural networks based SMC," *Materials Chemistry and Mechanics*, vol. 1, no. 4, pp. 31–39, 2023.
[33] M. Rahmani, "Control of a caterpillar robot manipulator using hybrid control," *Microsystem Technologies*, vol. 25, no. 7, pp. 2841–2854, 2019, doi: 10.1007/s00542-018-4280-9.
[34] A. Riani, T. Madani, A. Benallegue, and K. Djouani, "Adaptive integral terminal sliding mode control for upper-limb rehabilitation exoskeleton," *Control Engineering Practice*, vol. 75, pp. 108–117, 2018, doi: 10.1016/j.conengprac.2018.02.013.
[35] H. Wan *et al.*, "Toward universal embodied planning in scalable heterogeneous field robot collaboration and control," *Journal of Field Robotics*, vol. 42, no. 5, pp. 2318–2336, 2025, doi: 10.1002/rob.22522.

BIOGRAPHIES OF AUTHORS

Mai Hoang Nguyen received a Master's degree in Automation in 1998, and a PhD in Control Engineering and Automation in 2008 from Hanoi University of Science and Technology. Currently teaching at the Department of Automation - Faculty of Electrical Engineering, University of Science and Technology - University of Danang. Areas of interest: robots, power electronic converters, electric drives, power plant control, nonlinear control theory, measurement techniques. He can be contacted by phone at +84935283283 and by email at nhmai@dut.udn.vn.

Truc Thi Kim Nguyen received her Master degree at University of Ulsan, South Korea in 2013 and PhD. degree in Electrical and Information Engineering in Graz University of Technology, Austria in 2022. She is currently a researcher and lecturer at University of Science and Technology - The University of Danang, Da Nang, Vietnam. Her research focuses on machine learning and deep learning with application in various fields from image, video, time series data to medical audio signal processing. She can be contacted by phone at +84 975131812 and by email at ntktruc@dut.udn.vn.